Manipulating Au–CeO_2 Interfacial Structure Toward Ultrahigh Mass Activity and Selectivity for CO_2 Reduction

Jile Fu[+],[a, b, c] Dezhang Ren[+],[b] Meiling Xiao,[b] Ke Wang,[d] Yaping Deng,[b] Dan Luo,[b] Jianbing Zhu,[b] Guobin Wen,[b] Ying Zheng,*[c, d] Zhengyu Bai,*[a] Lin Yang,[a] and Zhongwei Chen*[b]

Deploying the application of Au-based catalysts directly on CO_2 reduction reactions (CO_2RR) relies on the simultaneous improvement of mass activity (usually lower than 10 mA mg$^{-1}_{Au}$ at −0.6 V) and selectivity. To achieve this target, we herein manipulate the interface of small-size Au (3.5 nm) and CeO_2 nanoparticles through adjusting the surface charge of Au and CeO_2. The well-regulated interfacial structure not only guarantees the utmost utilization of Au, but also enhances the CO_2 adsorption. Consequently, the mass activity (CO) of the optimal AuCeO_2/C catalyst reaches 139 mA mg$^{-1}_{Au}$ with 97% CO faradaic efficiency (FE_{CO}) at −0.6 V. Moreover, the strong interaction between Au and CeO_2 endows the catalyst with excellent long-term stability. This work affords a charge-guided approach to construct the interfacial structure for CO_2RR and beyond.

Introduction

In recent years, electrocatalytic CO_2 conversion has drawn great attention due to its ability to convert CO_2 to value-added products (CO,[1] formic acid,[2] ethylene,[3] etc) at ambient conditions. In order to improve the energy efficiency of this process, many catalysts were developed to achieve CO_2 reduction with high current density, high selectivity and low overpotential. In 1985, Hori et al.[4] investigated the catalytic behaviors of different groups of metals in the CO_2 electroreduction. Among all the metals studied, Au was the most promising metal that can produce CO.[5] Since then, extensive efforts have been made to modify Au-based materials towards boosted performance, including changing the oxidation state,[6] transforming the surface morphologies,[1a,7] alloying with other metals[8] and functionalizing the surface.[9] However, the reported mass activity (j_{CO}) is usually lower than 10 mA mg$^{-1}_{Au}$ at −0.6 V vs RHE.,[7c,10] which severely hinders the widespread application of Au-based materials due to the high expense of this noble metal. In this regard, improving the mass activity is highly desirable yet remains an immense challenge.

Typically, decreasing the particle size is an effective approach since only the surface atoms are active to CO_2RR.[11] Density functional theory (DFT) calculations also indicated that Au particle size has a significant influence on the affinity of the intermediate compounds (e.g., *COOH, *CO),[12] where CO_2 reduction rate with smaller Au particles is reported higher than that of the extended surface.[5b] Unfortunately, a similar trend was seen for the competing hydrogen evolution reaction (HER). Mistry et al.[13] investigated the size effect of Au on the CO_2 electroreduction. The activity of both HER and CO_2 reduction increase dramatically by orders of magnitudes with the decrease of Au particle size, whereas the total CO selectivity goes down. In order to achieve a high mass activity and high CO selectivity for small nanoparticles (<5 nm) of Au, an effective method must be used to either suppress the *H adsorption or improve the CO_2 adsorption.[14]

Metal-oxide interface has been used to improve the performance in many catalytic processes,[15] owing to its specific ability to activate molecule. Recently, Bao et al.[16] found that the hydroxyl group formed from the dissociation of H_2O is favored at Au–CeO_2 interface, which stabilizes the $CO_2^{\delta-}$ species. Thus, CO faradaic efficiency was greatly enhanced, and mass activity of Au reached 32.4 mA mg^{-1}Au at −0.89 V vs RHE. Although constructing Au–CeO_2 interface has been demonstrated to be effective to improve the catalytic selectivity, constructing enhanced metal-oxide interface without sacrificing the Au particle size is still challenging. In this work, we proposed an effective method to precisely control the interfacial structure of Au-based catalysts towards both high activity and selectivity, which was illustrated in Scheme 1. The pre-

[a] Dr. J. Fu,[+] Prof. Z. Bai, Prof. L. Yang
School of Chemistry and Chemical Engineering, Key Laboratory of Green Chemical Media and Reactions
Ministry of Education, Collaborative Innovation Center of Henan Province for Fine Chemicals Green Manufacturing
Henan Normal University
Xinxiang, 453007 (P. R. China)
E-mail: baizhengyu2000@163.com
[b] Dr. J. Fu,[+] Dr. D. Ren,[+] Dr. M. Xiao, Y. Deng, D. Luo, Dr. J. Zhu, G. Wen, Prof. Z. Chen
Department of Chemical Engineering, Waterloo Institute for Nanotechnology
Waterloo Institute for Sustainable Energy
University of Waterloo
Waterloo, Ontario N2 L 3G1 (Canada)
E-mail: zhwchen@uwaterloo.ca
[c] Dr. J. Fu,[+] Prof. Y. Zheng
Department of Chemical and Biochemical Engineering
Western University
London, Ontario, N6 A 5B9 (Canada)
E-mail: ying.zheng@uwo.ca
[d] Dr. K. Wang, Prof. Y. Zheng
Institute for Materials and Processes, School of Engineering
The University of Edinburgh
Edinburgh, EH9 3FB (UK)
[+] These authors contributed equally to this work.

Supporting information for this article is available on the WWW under https://doi.org/10.1002/cssc.202002133

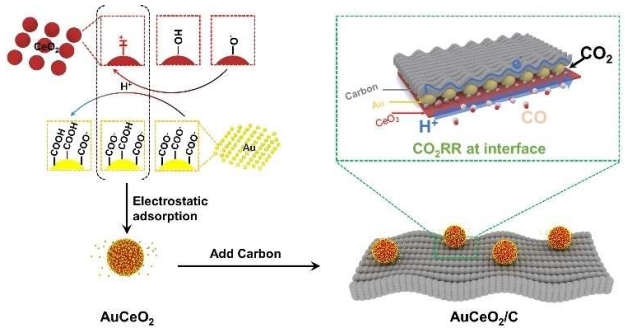

Scheme 1. Synthesis process of $AuCeO_2$/C.

synthesized Au and CeO_2 nanoparticles with adjustable surface charge were allowed to self-assemble through electrostatic adsorption process. Due to the strong electrostatic interaction, metal-oxide interface consisting of ultrafine Au nanoparticles and CeO_2 substrate was formed, which not only improved the utilization of Au atoms but also promoted CO_2 adsorption by interfacial synergy. As a result, the resultant $AuCeO_2$/C catalyst delivered ultrahigh Au mass activity (j_{CO}) of 139 mA mg^{-1}_{Au} and 97% CO faradaic efficiency at −0.6 V vs RHE.

Results and Discussion

Point of zero charge (PZC) is a specific pH of a solution, at which the metal oxide inside presents neutral surface hydroxyl. As shown in Figure 1a, when the pH is higher than PZC, hydroxyl groups that are populated on the oxide surface become deprotonated thereby negatively charged.[17] Conversely (pH < PZC), hydroxyl will be protonated, making the CeO_2 positively charged. On the other hand, the pH of the solution also affects the surface charge of Au nanoparticles, as Au is stabilized by sodium citrate. The terminal and tertiary carboxylate of citrate binds to the metal surface, while the second terminal carboxylate is unbound.[18] Thus, Au is negatively charged (R–COO^-). And, Au tends to be neutral with the decrease of pH, as the unbound carboxylate is converted to the carboxyl (Figure 1a, from R–COO^- to R–COOH). In order to obtain detailed information on the surface charge of Au and CeO_2, zeta potentials of both nanoparticles were measured under different pH conditions. As is shown in Figure1b, Au will repel CeO_2 at pH > 4, as both of them are strongly negative. Nevertheless, as pH declines to be lower than 2, many Au nanoparticles are neutralized, so that they are unable to be adsorbed on the positive CeO_2. Hence, there is a narrow pH window (2 < pH < 3), under which Au (negative) can automatically assemble on CeO_2 (positive) through electrostatic adsorption. The effect of pH on the composite of Au and CeO_2 nanoparticles further confirms the assembling process. At high pH (4.5–10), the zeta potential of the mixture (Au and CeO_2) is higher than that of Au nanoparticles but lower than that of CeO_2. This indicates the separation of these two types of nanoparticles, as the measurement mechanism is based on the counting of all the nanoparticles in the solution. As the pH declines to be lower than 3, a dramatic decrease of the zeta potential can be observed. This probably results from the assembling of Au and CeO_2 nanoparticles, companied by the conversion of carboxylate to carboxyl with the decrease of pH. The obtained composite tends to be neutral. When the pH is lower than 2, most of the Au nanoparticles would lose charge, while CeO_2 nanoparticles start to be positive. CeO_2 can hardly attract Au nanoparticles, thus the overall zeta potential of the Au–CeO_2 is slightly positive. Figure S1 presents the TEM images of Au and CeO_2 nanoparticles. Based on the zeta potential results, we investigated the effect of pH on the assembling of Au and CeO_2, which is shown in Figure 1c-f. The corresponding TEM images with higher resolution can be found in Figure S2 and S3. Obviously, Au and CeO_2 repel each other at pH = 4.5. With the decrease of pH, Au tends to be adsorbed on the surface of CeO_2. And $AuCeO_2$ composite was formed at pH = 2.8. However, with a further decrease of pH to 1.5, some Au nanoparticles are away from CeO_2 due to the partial neutralization of Au.

Figure 2a compares the XRD patterns of Au/C, $AuCeO_2$/C (pH = 2.8) and Au–CeO_2/C (pH = 3.5). Clearly, specific peaks that represent CeO_2 can be found in $AuCeO_2$/C and Au–CeO_2/C. Both the full width at half maximum (FWHM) and intensity of the peaks are similar between these two catalysts, demonstrating similar crystal structure and particle size of CeO_2 in these two catalysts. Besides, another peak located at 38° was also observed, which corresponds to the Au (111) plane. The sizes of Au were estimated to be 3.7 nm, 3.4 nm, and 3.5 nm for Au/C, $AuCeO_2$/C, and Au–CeO_2/C respectively (using Scherrer equation). To investigate the surface property of the as-synthesized catalysts, X-ray photoelectron spectroscopy (XPS) was recorded. In contrast to the XRD results, the intensity of Ce in $AuCeO_2$/C is much lower than that in Au–CeO_2/C (Figure S4, Ce3d spectra). In consideration of the analysis depth of XPS, which is around 3–9 nm, the main reason for the difference in intensity might be the different coverage of Au on CeO_2. This is consistent with the effect of pH on the assembling of Au and CeO_2 nanoparticles. Figure 2b shows the high-resolution Au 4f XPS spectra, revealing Au^0 for all the tested samples. Combining the XRD and XPS results, it can be concluded that the assembling process has a strong influence on the structure of $AuCeO_2$C, while the property of Au remains.

As is mentioned above, CO_2 adsorption is improved at metal-oxide interface.[16] Temperature programmed desorption (TPD) is employed to evaluate the CO_2 adsorption capacity, and the results are shown in Figure 2c. CeO_2 itself possesses an inferior capability of adsorbing CO_2. Au nanoparticles supported on carbon showed a small desorption peak at 450 °C, indicating a weak interaction with CO_2. A significant enhancement was observed with the addition of CeO_2, and this effect was strengthened from Au–CeO_2/C to $AuCeO_2$/C. The observation suggests that the capacity of a catalyst to adsorb CO_2 can be manipulated by changing the controllable combination of Au and CeO_2.

X-ray absorption fine-structure (XAFS) spectroscopy is an effective characterization method that provides both the

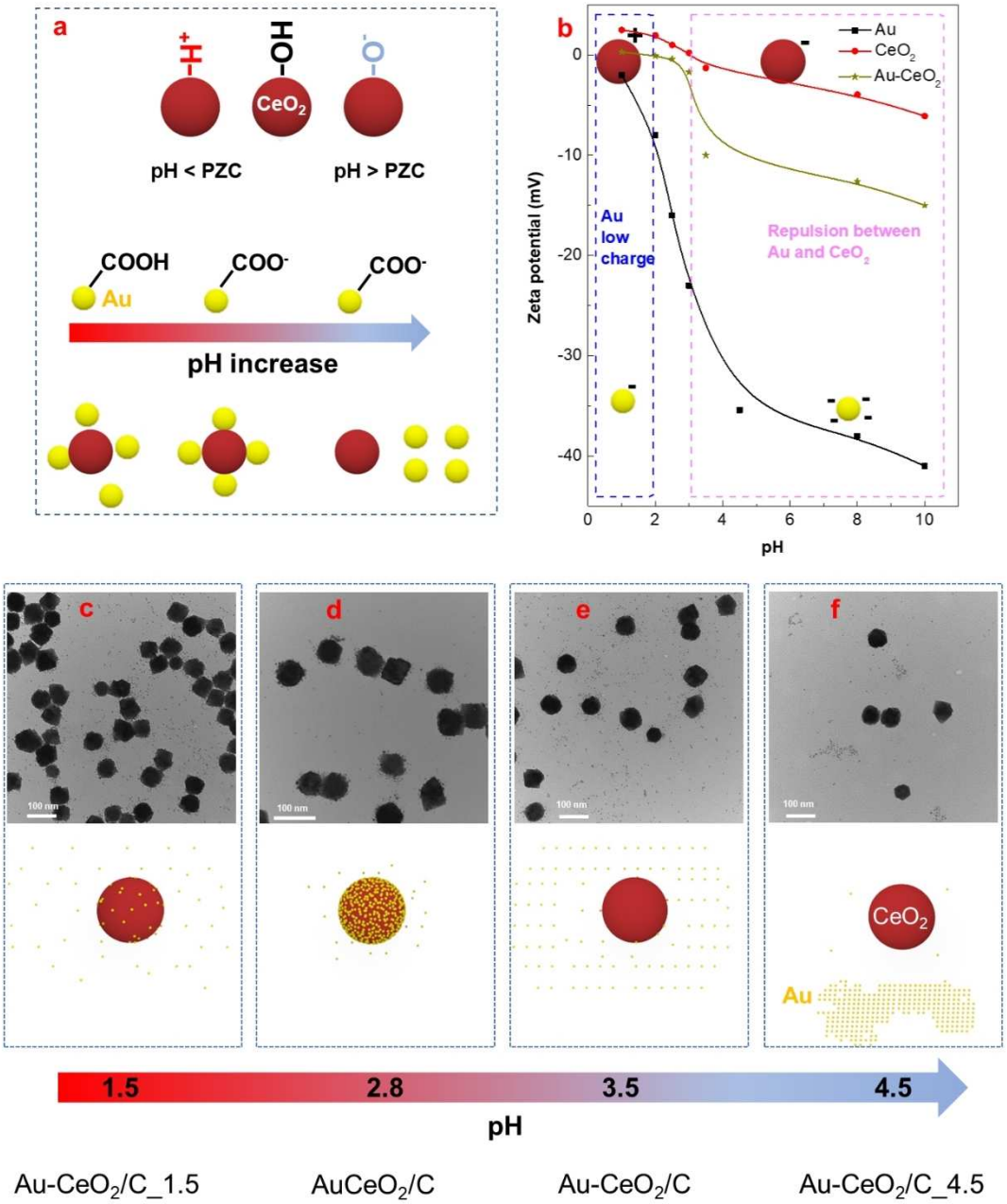

Figure 1. (a) Effect of pH on the surface charge of Au and CeO_2 particles and the electrostatic adsorption between them, (b) Zeta potential of Au, CeO_2 and Au–CeO_2 under different pH, (c–f) TEM images of Au and CeO_2 nanoparticles under different pH (scale bar 100 nm).

electronic property and crystallographic structure by X-ray absorption near-edge structure (XANES) and extended X-ray absorption fine structure (EXAFS), respectively. Figure 2d showed the XANES spectra of all the catalysts. The white line intensity indicates the Au $2p_{3/2}\rightarrow 5d$ transition,[19] which can be used to measure the oxidation state of Au. Obviously, no such prominent feature is observed in any of the samples that nanoparticles are present as metallic Au regardless of the support.[20] These results are consistent with XPS measurements. As is shown in the R space of the EXAFS results (Figure 2e), the major contribution for all the samples is the two peaks in R range from 2.2 Å to 3.2 Å. They are labelled as a single Au–Au single path, and the splitting results from the Ramsauer-Townsend resonance.[20] Another minor peak at ca. 2.1 Å was attributable to Au–O scattering path, which resulted from the covalent bonding between gold atoms and oxygen atoms of the support and thus longer than that of the Au–O distance in Au_2O_3.[21] Au/CeO_2 exhibited much higher Au–O intensity than Au/C did due to the metallic state of Au (confirmed by XPS and XANES). Notably, Au–O contribution for $AuCeO_2$/C is signifi-

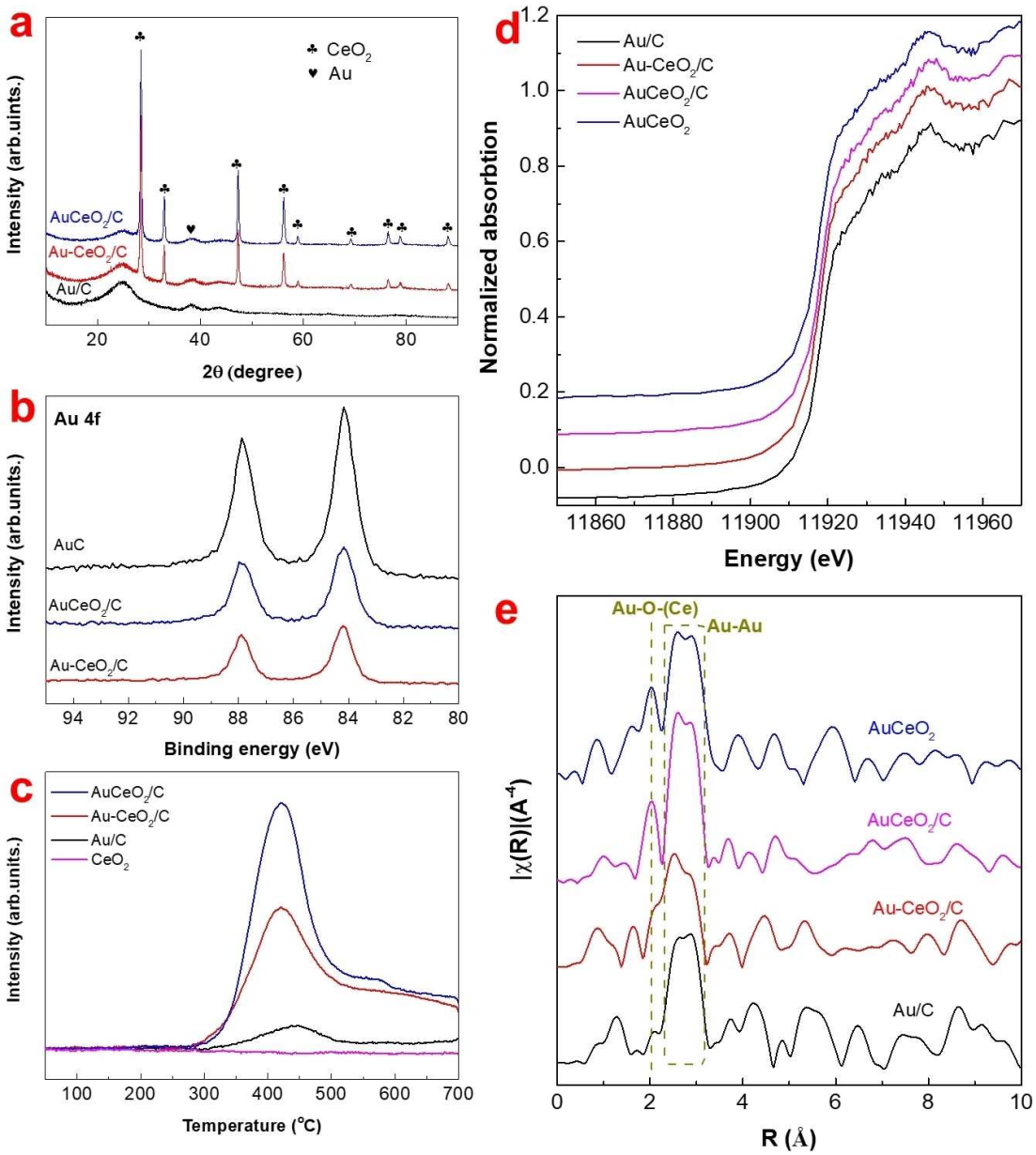

Figure 2. (a) XRD patterns of Au/C, $AuCeO_2$/C and Au–CeO_2/C, (b) High-resolution XPS spectra of Au/C, $AuCeO_2$/C, Au–CeO_2/C, (c) Temperature programmed desorption of CO_2 results, (d) XANES spectra of Au/C, $AuCeO_2$/C, Au–CeO_2/C and $AuCeO_2$, (e) EXAFS data of Au/C, $AuCeO_2$/C, Au–CeO_2/C and $AuCeO_2$.

cantly increased, much higher than that of Au–CeO_2/C, which is ascribed to the enhanced interaction between Au and CeO_2. Thus, we can establish that Au nanoparticles are located on CeO_2 in $AuCeO_2$/C, creating the enhanced metal-oxide interface.

A representative transmission electron microscopy (TEM) image of Au/C is displayed in Figure S5. The statistic size of Au is 3.6 nm, matching well with the calculated Au size from XRD. The high-resolution TEM (HRTEM) image showed the d-spacing of Au (111), which is confirmed by the fast fourier transform (FFT) image. To further investigate the catalyst structure, high angle annular dark field (HAADF) scanning transmission electron microscopy (STEM) and elemental mapping were performed. The results of $AuCeO_2$/C are shown in Figure 3. Clearly, Au nanoparticles with 3–4 nm were selectively located on the CeO_2 nanoparticles. HRTEM images present the lattice of CeO_2 (111) and Au (111) at Au–CeO_2 interface. In contrast to $AuCeO_2$/C, a large amount of Au and CeO_2 nanoparticles are separately deposited on carbon for Au–CeO_2/C, which is apparent in the HADDF-STEM and elemental mappings images (Figure S7). The corresponding HRTEM image presents a clear boundary between Au and CeO_2 nanoparticles.

The performance of carbon, CeO_2, $AuCeO_2$, Au/C was evaluated respectively in CO_2RR, and the results are shown in Figure 4a and 4b. Only gas products were detected, which has been confirmed by nuclear magnetic resonance (NMR) and gas chromatography (GC). The current density of carbon is lower

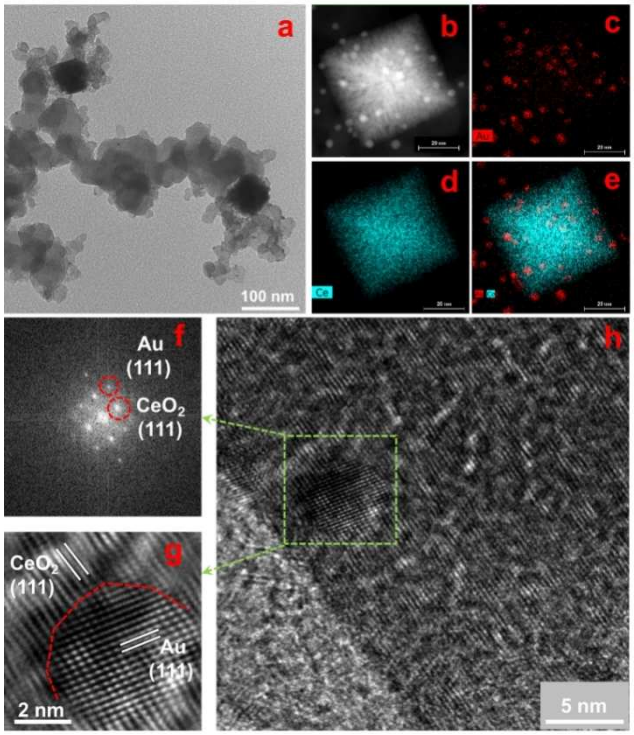

Figure 3. (a) TEM image of $AuCeO_2$/C, (b) HAADF-STEM image of $AuCeO_2$/C, (c) Elemental EDS mapping results of Au, (d) Elemental EDS mapping results of Ce, (e) Overlayer of Au and Ce EDS mappings, (f) FFT patterns, (g) HRTEM of Au and CeO_2 in $AuCeO_2$/C, (h) HRTEM image of $AuCeO_2$/C.

than 1 mA cm^{-2} at −0.5 V and 0.6 V. As the applied potential increases to −0.7 V, a dramatic rise of the activity is obtained. Nevertheless, the main product for carbon is H_2. Both CeO_2 and $AuCeO_2$ exhibit much lower current density than carbon does, which is attributed to the low conductivity of CeO_2. By contrast, the CO faradaic efficiency (FE_{CO}) of $AuCeO_2$ reaches 83% at −0.8 V. Au/C presents the highest current density, and the FE_{CO} increases gradually with the applied potential. Based on these results, we can conclude that Au is the active site where CO_2RR occurs. The combination of Au and CeO_2 improves the FE_{CO}, but the current density is too low.

Inspired by the desirable metal-oxide interfacial structure, we investigated the electrocatalytic CO_2RR properties of the $AuCeO_2$/C and Au–CeO_2/C catalysts. Figure 4c and 4d present the performance of catalysts prepared under different pH (pH = 1.5, 2.8, 3.5, 4.5) in CO_2RR. Clearly, a strong dependency of catalysts structure on the final current density and FE_{CO} was observed. As is shown in Figure 1 and Figure S2, the number of Au nanoparticles that were assembled on CeO_2 follows the order: $AuCeO_2$/C > Au–CeO_2/C_1.5 > Au–CeO_2/C > Au–CeO_2/C_4.5. At low potentials (−0.5 to −0.7 V), the current density of these catalysts follows the same order, which confirms the importance of Au–CeO_2 interface for CO_2 reduction. As the applied potential is higher than −0.7 V, the activity of Au–CeO_2/C_4.5 is slightly higher than that of Au–CeO_2/C. The main reason should be the enhanced CO_2RR and HER activity of Au nanoparticles at high potential, which has been shown in Figure 4a and 4b. Nevertheless, $AuCeO_2$/C presents the highest current density at overall potentials. By contrast, the FE_{CO} of theses catalysts increases gradually with the Au–CeO_2 interface. The FE_{CO} of $AuCeO_2$/C is 91% and 97% under −0.5 V and −0.6 V respectively (0.5 M $KHCO_3$). An obvious gap of linear sweep voltammetry (LSV) plots between N_2 and CO_2 saturated electrolytes for $AuCeO_2$/C is observed, indicating the vital role CO_2 adsorption (Figure S8) in the CO_2RR. Using 0.1 M $KHCO_3$ makes the FE_{CO} a little lower, but it can still reach 90% at −0.6 V (Figure S9). By contrast, Au–CeO_2/C shows much lower FE_{CO} at −0.5 V, which is only 48% using 0.1 M $KHCO_3$ and 65% at 0.5 M (Figure S10). Only after the potential is over −0.8 V can the FE_{CO} of Au–CeO_2/C reach 90% with 0.5 M $KHCO_3$. The situation is even worse using Au–CeO_2/C_4.5 which has the least Au–CeO_2 interface.

As the loading of Au is only 0.04 mg/cm^2, the mass activity of $AuCeO_2$/C goes up to 139 mA/mg$_{Au}$ at −0.6 V (Figure 5a). Figure 5b compares the performance of $AuCeO_2$/C catalysts with the reported Au based catalysts. The mass activity of Au nanoparticles is usually lower than 10 mA/mg at −0.6 V. The conventional size or shape control method of Au is inefficient in terms of both high mass activity and selectivity, unless alloying with other metal.[22] The self-assembly strategy proposed in this work breaks the limitation of Au, and superior performance was achieved. The stability of $AuCeO_2$/C was tested at −0.6 V for 24 h (Figure 5c). During the process, both FE_{CO} and mass activity of $AuCeO_2$/C remained stable.

As noted above, small-size Au tends to generate high current density at the expense of accelerated HER competing reaction, resulting in low FE_{CO}. In all the tested samples, the average size of Au nanoparticles was estimated to be 3.5 nm by TEM and XRD. Despite the small particle size, $AuCeO_2$/C presents a significant increase in FE_{CO}, accompanied with a high current density. The structural analysis and TPD results suggest that both the strength and density of CO_2 adsorption are improved owing to the significant Au–CeO_2 interface created. Thus, electrons that were transferred to the active sites would preferentially react with CO_2 thereby suppressing the HER. For Au–CeO_2/C, FE_{CO} is lower than that of $AuCeO_2$/C, which is attributed to the low Au–CeO_2 interface.

Conclusions

A self-assembly strategy utilizing electrostatic interaction has been developed to synthesize the $AuCeO_2$/C catalysts with controllable metal-oxide interfacial structure. The assembling of pre-synthesized Au and CeO_2 nanoparticles was achieved by precisely controlling their surface charge. With the well-regulated surface charge, Au particles (small size) can be selectively anchored on the CeO_2 surface to form enhanced metal-oxide interface. Consequently, a significant enhancement for FE_{CO} was observed at low potentials, and the mass activity (CO) of Au reaches 139 mA/mg at −0.6 V. This work clearly indicates the structure-dependent catalytic performance in CO_2 reduction. The assembling of nanoparticles by adjusting their surface charge can be extended for the construction of

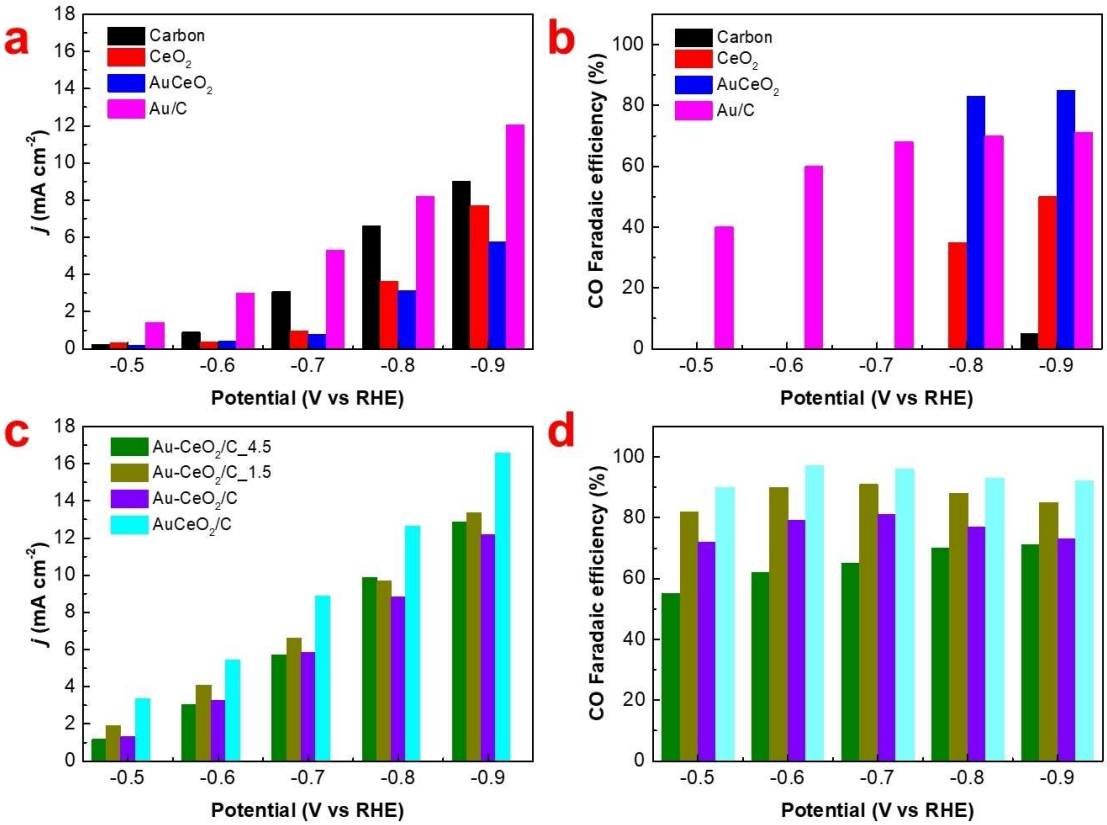

Figure 4. (a, b) Comparison of the potential-dependent performance of carbon, CeO_2, $AuCeO_2$ and Au/C under 0.5 M $KHCO_3$. The CO faradaic efficiency for CeO_2 and $AuCeO_2$ is not shown at −0.5 V, −0.6 V and −0.7 V due to the low current density. (c, d) Comparison of the potential-dependent performance of $AuCeO_2$/C, Au–CeO_2/C, Au–CeO_2/C_1.5, Au–CeO_2/C_4.5 under 0.5 M $KHCO_3$.

desirable interfacial structure with tailored catalytic performance.

Experimental Section

Chemicals

$NaBH_4$ (98%), KCl (99.5%), $KHCO_3$ (99.7%), $HAuCl_4$ (99%), PVP (Mw = 360000), Nafion resin solution (5 wt% in a mixture of lower aliphatic alcohols & H_2O), cerium nitrate hexahydrate (99%), sodium citrate dihydrate (99%), ethanol (95%) and HCl (37%) were purchased from Sigma-Aldrich. Gas diffusion layer (GDL 29BC) was purchased from ion power. Vulcan XC-72R was purchased from FuelCellStore.

Catalysts preparation

Au nanoparticles were synthesized using chemical reduction method. Typically, the $HAuCl_4$ solution (1 mg Au/mL water), sodium citrate solution (10 mg/mL), and $NaBH_4$ (0.1 M) were prepared. Then, sodium citrate was added in the $HAuCl_4$ solution with stirring. 5 min later, $NaBH_4$ ($NaBH_4$/Au mole fraction = 4) solution was added which made solution dark brown. After 30 min, the Au nanoparticles were stored for further use.

CeO_2 nanoparticles were prepared by hydrothermal method.[23] Cerium nitrate hexahydrate (0.85 g) was added into the mixture of deionized water (5 mL) and ethanol (5 mL). Then, PVP solution (1.8 g PVP in 30 mL deionized water) was prepared and mixed with the cerium nitrate solution. After that, the obtained mixture was transferred into a stainless-steel autoclave and heated to 140 °C for 24 h. The as-synthesized CeO_2 particles were separated by centrifugation (11000 rpm, 1 h), followed by twice wash with water and ethanol (8000 rpm, 40 min). Finally, the CeO_2 nanoparticles were dispersed in ethanol (5 mg/mL ethanol).

$AuCeO_2$/C was prepared by post-assembly method. The colloidal Au (1 mg) and CeO_2 (10 mg) were added into deionized water (100 mL). Then, HCl (3.5%) solution was added to adjust the pH (2.8), followed by vigorous stirring for 1 h. After that, carbon (Vulcan XC-72R, 39 mg) was added with sonication for 5 min and stirring for 1 h. The as-synthesized catalyst was collected by centrifugation (8500 rpm, 10 min), washed with deionized water and dried in oven at 70 °C for 8 h. Au–CeO_2/C were synthesized by a similar method, except that the pH was 3.5.

Au/C was prepared by depositing the Au nanoparticles on carbon as follows: 49 mg carbon (Vulcan XC-72R) was dispersed in H_2O using ultrasonic machine for 5 min. Then, Au nanoparticles (1 mg Au) was added, followed by pH adjustment to be 2.8 with HCl (3.5%). The obtained catalyst was collected by filtration and dried in oven at 70 °C for 8 h. $AuCeO_2$ was prepared by a similar method, in which carbon was replaced by CeO_2. The as-synthesized catalyst was collected by centrifugation, washed with deionized water and dried in the oven.

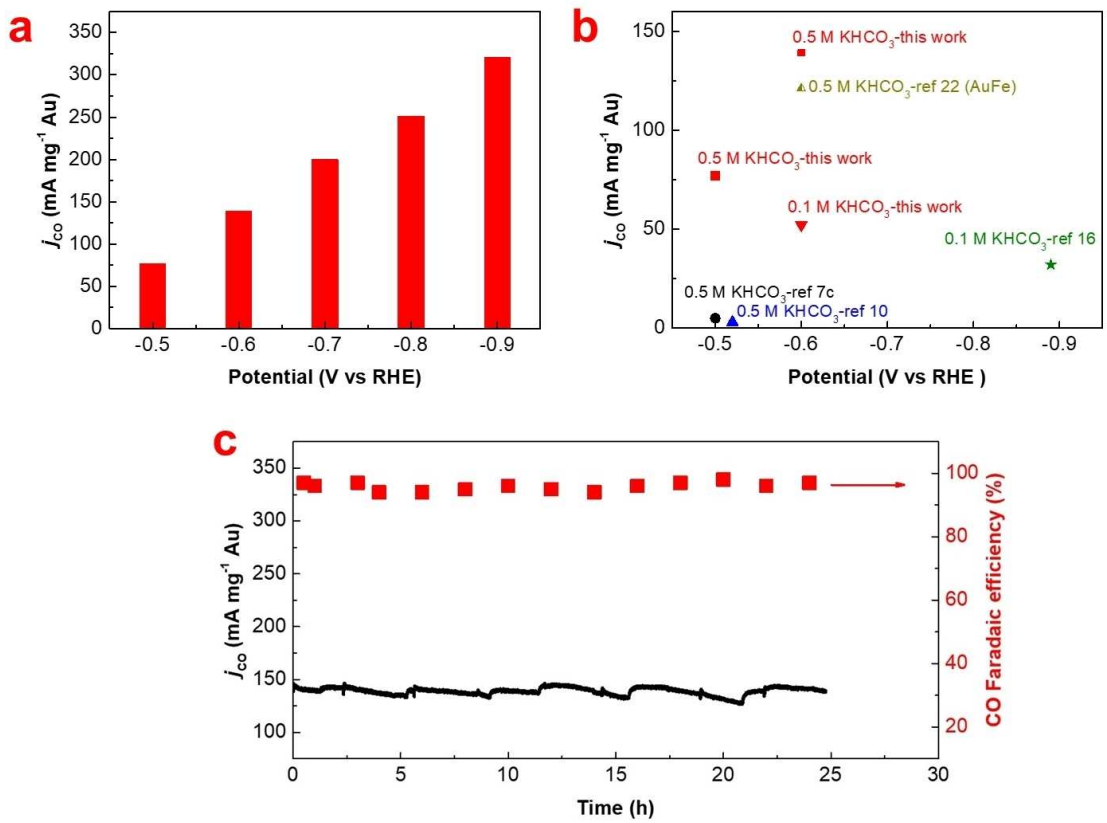

Figure 5. (a) Mass activity at designated potentials obtained for $AuCeO_2$/C under 0.5 M $KHCO_3$, (b) Activity of Au catalysts in this work compared with the Au based catalysts in the references, (c) Long-term stability test of $AuCeO_2$/C at −0.6 V.

Electrode preparation

Electrode was prepared by panting the catalysts on the carbon paper with gas diffusion layer (GDL 29BC, Ion Power). First, Nafion ionomer solution (5%), catalyst and ethanol were mixed by sonification for 20 min. Then, the obtained catalyst ink was sprayed on the carbon paper at 75 °C, with total catalyst loading 2 mg cm^{-2}. Thus, the Au loading is 0.04 mg cm^{-2}.

Electrochemical measurements

CO_2 electrochemical reduction reaction (CO_2RR) was conducted in a three-electrode cell with Nafion 117 membrane to separate the two compartments. Pt wire was utilized as counter electrode, while saturated calomel electrode (SCE) works as reference electrode. A potentiostat (Gamry-Interface 5000E) was used for all the electrochemical measurements. The measured potentials were converted to the RHE reference scale according to formula: E (RHE) = E (SCE) + 0.235 V + 0.0591 × pH. CO_2RR was operated in CO_2-saturated 0.1 M (pH = 6.8) or 0.5 M (pH = 7.2) $KHCO_3$. The gas product was analyzed by gas chromatography equipped with HID detector and HayeSep packed column. The liquid products (e.g., formate or methanol) were detected using a 500 M ^{1}H liquid NMR spectrometer. The conversion of J_{CO} (mA mg^{-1} Au) to J_{CO} (mA cm^{-2}) follows Equation (1) below:

$$J_{CO}\ (\mathrm{mA\,cm^{-2}}) = J_{CO}\ (\mathrm{mA\,mg^{-1}\ Au}) \times 0.04 \quad (1)$$

Physicochemical characterization

X-ray diffraction (XRD) was performed on Rigaku Miniflex 600 at 40 kV and 200 mA. X-ray photoelectron spectroscopy analysis was carried on thermal scientific K-α spectrometer. Zeta potential was measured using Nano ZS90 Malvern with folded capillary cell. Transmission electron microscopy (TEM) images were obtained from JEOL 2010F. Spectra of X-ray absorption fine-structure (XAFS) spectroscopy were collected using the beamline BioXAS spectroscopy of Canadian Light Source.

Temperature programmed desorption of CO_2 (CO_2-TDP) was carried with an AMI-200 instrument. Catalyst (60 mg) was firstly treated by helium (30 mL min^{-1}) at 150 °C for 1 h, and cooled down to 50 °C. Then, CO_2 adsorption was performed at 50 °C for 0.5 h (CO_2, 30 mL min^{-1}). After that, catalyst was purged by helium (30 mL min^{-1}) for 0.5 h at 50 °C, followed by the CO_2 desorption in flowing helium (30 mL min^{-1}) from 50 to 500 °C at a heating rate of 10 °C min^{-1}. The signal of CO_2 was collected by mass spectrometer connected on-line.

Acknowledgements

This work was supported by National Natural Science Foundation of China (Grant No. 51922008 and 51872075), the 111 Project (Grant No. D17007), Henan Center for Outstanding Overseas Scientists (Grant No. GZS2018003), and the University of Waterloo. The authors also thank Dr. Shuang Li from Brookhaven National

Laboratory (USA) for Transmission electron microscopy measurements, Dr. Chau Mai from University of Waterloo for CO_2-TPD measurements, and thank Dr. Yongfeng Hu, Dr. Qunfeng Xiao, Dr. Roman Chernikov, Dr. David Muir, Dr. Mohsen Shakouri from Canadian Light Source (CLS) for XAS measurements. The CLS is supported by the NSERC, the National Research Council Canada, the Canadian Institutes of Health Research, the Province of Saskatchewan, Western Economic Diversification Canada, and the University of Saskatchewan.

Conflict of Interest

The authors declare no conflict of interest.

Keywords: CO_2 reduction reactions · Interface manipulation · Surface charge · CO_2 adsorption · $AuCeO_2$/C

[1] a) R. G. Mariano, K. McKelvey, H. S. White, M. W. Kanan, *Science* **2017**, *358*, 1187–1192; b) J. Gu, C.-S. Hsu, L. Bai, H. M. Chen, X. Hu, *Science* **2019**, *364*, 1091–1094; c) J. Liu, L. Peng, Y. Zhou, L. Lv, J. Fu, J. Lin, D. Guay, J. Qiao, *ACS Sustainable Chem. Eng.* **2019**, *7*, 15739–15746; d) S. Lin, C. S. Diercks, Y.-B. Zhang, N. Kornienko, E. M. Nichols, Y. Zhao, A. R. Paris, D. Kim, P. Yang, O. M. Yaghi, C. J. Chang, *Science* **2015**, *349*, 1208–1213; e) Y. Hori, H. Wakebe, T. Tsukamoto, O. Koga, *Electrochim. Acta* **1994**, *39*, 1833–1839; f) M. Asadi, K. Kim, C. Liu, A. V. Addepalli, P. Abbasi, P. Yasaei, P. Phillips, A. Behranginia, J. M. Cerrato, R. Haasch, P. Zapol, B. Kumar, R. F. Klie, J. Abiade, L. A. Curtiss, A. Salehi-Khojin, *Science* **2016**, *353*, 467–470; g) S. Ringe, E. L. Clark, J. Resasco, A. Walton, B. Seger, A. T. Bell, K. Chan, *Energy Environ. Sci.* **2019**, *12*, 3001–3014; h) J. Han, P. An, S. Liu, X. Zhang, D. Wang, Y. Yuan, J. Guo, X. Qiu, K. Hou, L. Shi, Y. Zhang, S. Zhao, C. Long, Z. Tang, *Angew. Chem. Int. Ed.* **2019**, *58*, 12711–12716; *Angew. Chem.* **2019**, *131*, 12841–12846; i) L. Sun, V. Reddu, A. C. Fisher, X. Wang, *Energy Environ. Sci.* **2020**, *13*, 374–403; j) Z. Yang, X. Zhang, C. Long, S. Yan, Y. Shi, J. Han, J. Zhang, P. An, L. Chang, Z. Tang, *CrystEngComm* **2020**, *22*, 1619–1624.

[2] a) X. Zhang, X. Hou, Q. Zhang, Y. Cai, Y. Liu, J. Qiao, *J. Catal.* **2018**, *365*, 63–70; b) G. Wen, D. U. Lee, B. Ren, F. M. Hassan, G. Jiang, Z. P. Cano, J. Gostick, E. Croiset, Z. Bai, L. Yang, Z. Chen, *Adv. Energy Mater.* **2018**, *8*, 1802427; c) M. Wang, N. Preston, N. Xu, Y. Wei, Y. Liu, J. Qiao, *ACS Appl. Mater. Interfaces* **2019**, *11*, 6881–6889; d) L. Peng, Y. Wang, I. Masood, B. Zhou, Y. Wang, J. Lin, J. Qiao, F.-Y. Zhang, *Appl. Catal. B.* **2020**, *264*, 118447; e) Q. Zhang, Y. Zhang, J. Mao, J. Liu, Y. Zhou, D. Guay, J. Qiao, *ChemSusChem* **2019**, *12*, 1443–1450; f) S. Zhao, S. Li, T. Guo, S. Zhang, J. Wang, Y. Wu, Y. Chen, *Nano-Micro Lett.* **2019**, *11*, 62.

[3] a) C.-T. Dinh, T. Burdyny, M. G. Kibria, A. Seifitokaldani, C. M. Gabardo, F. P. García de Arquer, A. Kiani, J. P. Edwards, P. De Luna, O. S. Bushuyev, C. Zou, R. Quintero-Bermudez, Y. Pang, D. Sinton, E. H. Sargent, *Science* **2018**, *360*, 783–787; b) T.-C. Chou, C.-C. Chang, H.-L. Yu, W.-Y. Yu, C.-L. Dong, J.-J. Velasco-Vélez, C.-H. Chuang, L.-C. Chen, J.-F. Lee, J.-M. Chen, H.-L. Wu, *J. Am. Chem. Soc.* **2020**, *142*, 2857–2867; c) Y. Gao, Q. Wu, X. Liang, Z. Wang, Z. Zheng, P. Wang, Y. Liu, Y. Dai, M.-H. Whangbo, B. Huang, *Adv. Sci.* **2019**, *29*, 1902820; d) J. Kim, W. Choi, J. W. Park, C. Kim, M. Kim, H. Song, *J. Am. Chem. Soc.* **2019**, *141*, 6986–6994; e) F. Li, A. Thevenon, A. Rosas-Hernández, Z. Wang, Y. Li, C. M. Gabardo, A. Ozden, C. T. Dinh, J. Li, Y. Wang, J. P. Edwards, Y. Xu, C. McCallum, L. Tao, Z.-Q. Liang, M. Luo, X. Wang, H. Li, C. P. O'Brien, C.-S. Tan, D.-H. Nam, R. Quintero-Bermudez, T.-T. Zhuang, Y. C. Li, Z. Han, R. D. Britt, D. Sinton, T. Agapie, J. C. Peters, E. H. Sargent, *Nature* **2020**, *577*, 509–513; f) H. Mistry, A. S. Varela, C. S. Bonifacio, I. Zegkinoglou, I. Sinev, Y.-W. Choi, K. Kisslinger, E. A. Stach, J. C. Yang, P. Strasser, B. R. Cuenya, *Nat. Commun.* **2016**, *7*, 12123.

[4] H. Yoshio, K. Katsuhei, S. Shin, *Chem. Lett.* **1985**, *14*, 1695–1698.

[5] a) A. A. Peterson, J. K. Nørskov, *J. Phys. Chem. Lett.* **2012**, *3*, 251–258; b) S. Mezzavilla, S. Horch, I. E. L. Stephens, B. Seger, I. Chorkendorff, *Angew. Chem. Int. Ed.* **2019**, *58*, 3814–3818; *Angew. Chem.* **2019**, *131*, 3854–3858.

[6] Y. Chen, C. W. Li, M. W. Kanan, *J. Am. Chem. Soc.* **2012**, *134*, 19969–19972.

[7] a) M. Liu, Y. Pang, B. Zhang, P. De Luna, O. Voznyy, J. Xu, X. Zheng, C. T. Dinh, F. Fan, C. Cao, F. P. G. de Arquer, T. S. Safaei, A. Mepham, A. Klinkova, E. Kumacheva, T. Filleter, D. Sinton, S. O. Kelley, E. H. Sargent, *Nature* **2016**, *537*, 382; b) X. Feng, K. Jiang, S. Fan, M. W. Kanan, *J. Am. Chem. Soc.* **2015**, *137*, 4606–4609; c) W. Zhu, Y.-J. Zhang, H. Zhang, H. Lv, Q. Li, R. Michalsky, A. A. Peterson, S. Sun, *J. Am. Chem. Soc.* **2014**, *136*, 16132–16135.

[8] a) X. Yuan, L. Zhang, L. Li, H. Dong, S. Chen, W. Zhu, C. Hu, W. Deng, Z.-J. Zhao, J. Gong, *J. Am. Chem. Soc.* **2019**, *141*, 4791–4794; b) D. Kim, C. Xie, N. Becknell, Y. Yu, M. Karamad, K. Chan, E. J. Crumlin, J. K. Nørskov, P. Yang, *J. Am. Chem. Soc.* **2017**, *139*, 8329–8336.

[9] a) Z. Cao, D. Kim, D. Hong, Y. Yu, J. Xu, S. Lin, X. Wen, E. M. Nichols, K. Jeong, J. A. Reimer, P. Yang, C. J. Chang, *J. Am. Chem. Soc.* **2016**, *138*, 8120–8125; b) D. R. Kauffman, D. Alfonso, C. Matranga, H. Qian, R. Jin, *J. Am. Chem. Soc.* **2012**, *134*, 10237–10243; c) Y. Fang, J. C. Flake, *J. Am. Chem. Soc.* **2017**, *139*, 3399–3405.

[10] W. Zhu, R. Michalsky, Ö. Metin, H. Lv, S. Guo, C. J. Wright, X. Sun, A. A. Peterson, S. Sun, *J. Am. Chem. Soc.* **2013**, *135*, 16833–16836.

[11] L. Jin, B. Liu, P. Wang, H. Yao, L. A. Achola, P. Kerns, A. Lopes, Y. Yang, J. Ho, A. Moewes, Y. Pei, J. He, *Nanoscale* **2018**, *10*, 14678–14686.

[12] C. Shi, H. A. Hansen, A. C. Lausche, J. K. Nørskov, *Phys. Chem. Chem. Phys.* **2014**, *16*, 4720–4727.

[13] H. Mistry, R. Reske, Z. Zeng, Z.-J. Zhao, J. Greeley, P. Strasser, B. R. Cuenya, *J. Am. Chem. Soc.* **2014**, *136*, 16473–16476.

[14] X. Zhang, H. Liu, Y. Shi, J. Han, Z. Yang, Y. Zhang, C. Long, J. Guo, Y. Zhu, X. Qiu, G. Xue, L. Zhang, B. Zhang, L. Chang, Z. Tang, *Matter* **2020**, *3*, 558–570.

[15] a) Y. Suchorski, S. M. Kozlov, I. Bespalov, M. Datler, D. Vogel, Z. Budinska, K. M. Neyman, G. Rupprechter, *Nat. Mater.* **2018**, *17*, 519–522; b) Q. Fu, F. Yang, X. Bao, *Acc. Chem. Res.* **2013**, *46*, 1692–1701; c) J. Saavedra, H. A. Doan, C. J. Pursell, L. C. Grabow, B. D. Chandler, *Science* **2014**, *345*, 1599–1602; d) S. Kattel, P. Liu, J. G. G. Chen, *J. Am. Chem. Soc.* **2017**, *139*, 9739–9754; e) J. Graciani, K. Mudiyanselage, F. Xu, A. E. Baber, J. Evans, S. D. Senanayake, D. J. Stacchiola, P. Liu, J. Hrbek, J. F. Sanz, J. A. Rodriguez, *Science* **2014**, *345*, 546–550; f) S. W. Li, Y. Xu, Y. F. Chen, W. Z. Li, L. L. Lin, M. Z. Li, Y. C. Deng, X. P. Wang, B. H. Ge, C. Yang, S. Y. Yao, J. L. Xie, Y. W. Li, X. Liu, D. Ma, *Angew. Chem. Int. Ed.* **2017**, *56*, 10761–10765; *Angew. Chem.* **2017**, *129*, 10901–10905; g) X. Yang, S. Kattel, S. D. Senanayake, J. A. Boscoboinik, X. Nie, J. Graciani, J. A. Rodriguez, P. Liu, D. J. Stacchiola, J. G. Chen, *J. Am. Chem. Soc.* **2015**, *137*, 10104–10107.

[16] D. Gao, Y. Zhang, Z. Zhou, F. Cai, X. Zhao, W. Huang, Y. Li, J. Zhu, P. Liu, F. Yang, G. Wang, X. Bao, *J. Am. Chem. Soc.* **2017**, *139*, 5652–5655.

[17] L. Jiao, J. R. Regalbuto, *J. Catal.* **2008**, *260*, 329–341.

[18] C. H. Munro, W. E. Smith, M. Garner, J. Clarkson, P. C. White, *Langmuir* **1995**, *11*, 3712–3720.

[19] G. Malta, S. A. Kondrat, S. J. Freakley, C. J. Davies, L. Lu, S. Dawson, A. Thetford, E. K. Gibson, D. J. Morgan, W. Jones, P. P. Wells, P. Johnston, C. R. A. Catlow, C. J. Kiely, G. J. Hutchings, *Science* **2017**, *355*, 1399–1403.

[20] W. Deng, A. I. Frenkel, R. Si, M. Flytzani-Stephanopoulos, *J. Phys. Chem. C* **2008**, *112*, 12834–12840.

[21] a) A. M. Argo, J. F. Odzak, F. S. Lai, B. C. Gates, *Nature* **2002**, *415*, 623–626; b) L. Delannoy, N. Weiher, N. Tsapatsaris, A. M. Beesley, L. Nchari, S. L. M. Schroeder, C. Louis, *Top. Catal.* **2007**, *44*, 263–273; c) J. Guzman, S. Carrettin, J. C. Fierro-Gonzalez, Y. Hao, B. C. Gates, A. Corma, *Angew. Chem. Int. Ed.* **2005**, *44*, 4778–4781; *Angew. Chem.* **2005**, *117*, 4856–4859.

[22] K. Sun, T. Cheng, L. Wu, Y. Hu, J. Zhou, A. Maclennan, Z. Jiang, Y. Gao, W. A. Goddard, Z. Wang, *J. Am. Chem. Soc.* **2017**, *139*, 15608–15611.

[23] J. Su, C. Xie, C. Chen, Y. Yu, G. Kennedy, G. A. Somorjai, P. Yang, *J. Am. Chem. Soc.* **2016**, *138*, 11568–11574.

Manuscript received: September 8, 2020
Revised manuscript received: October 16, 2020
Accepted manuscript online: October 26, 2020
Version of record online: ■■, ■■■

FULL PAPERS

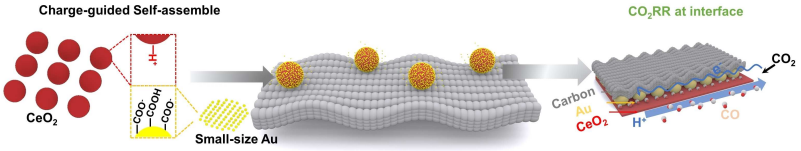

Putting Au to good use: The charge-guided assembling of Au and CeO_2 nanoparticles creates an enhanced Au–CeO_2 interface and guarantees the outmost utilization of Au. Thus, both high activity and CO selectivity were achieved.

Dr. J. Fu, Dr. D. Ren, Dr. M. Xiao, Dr. K. Wang, Y. Deng, D. Luo, Dr. J. Zhu, G. Wen, Prof. Y. Zheng, Prof. Z. Bai*, Prof. L. Yang, Prof. Z. Chen**